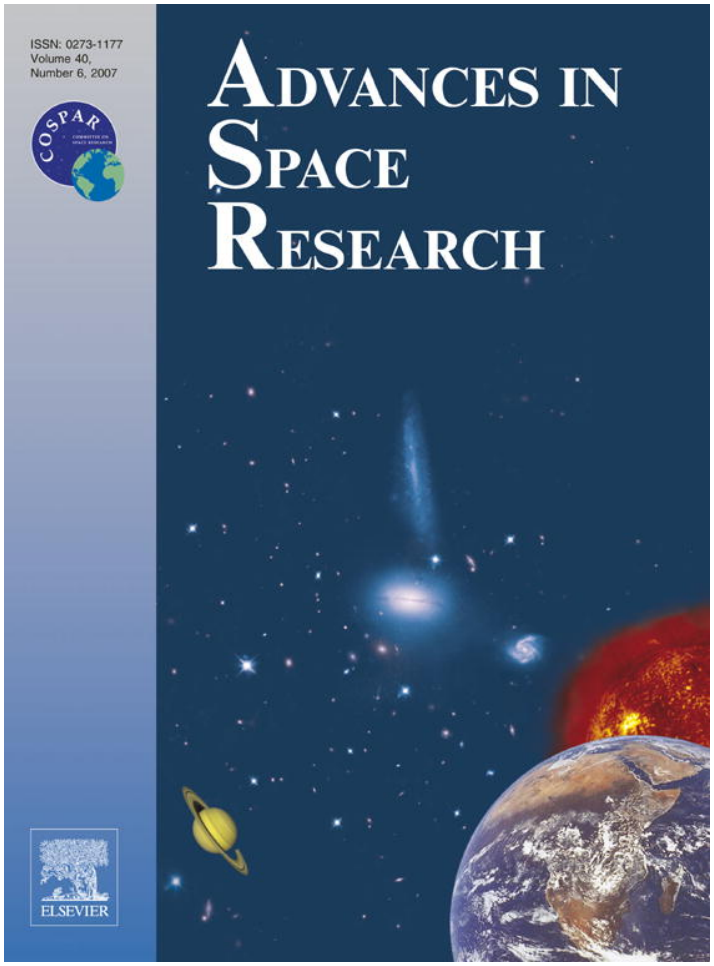

Available online at www.sciencedirect.com
ScienceDirect
Advances in Space Research 40 (2007) 785–793
ADVANCES IN SPACE RESEARCH (a COSPAR publication)
www.elsevier.com/locate/asr

Simultaneous observations of temperatures and ice-particles in the mid-latitude mesopause region

Michael Gerding *, Josef Höffner, Monika Rauthe

Leibniz Institute of Atmospheric Physics, Schlossstr. 6, 18225 Kühlungsborn, Germany

Received 1 November 2006; received in revised form 5 January 2007; accepted 8 January 2007

Abstract

At the mid-latitude location of Kühlungsborn (54°N, 12°E) a number of noctilucent clouds (NLC) have been observed in the last years by ground-based lidars. Since 1997 up to five NLC per year have been detected (occurrence rate up to 12%), showing that the atmospheric conditions for NLC are fulfilled only occasionally at this location. The mean NLC altitude is 83.0 km and the mean NLC backscatter coefficient at 532 nm wavelength is about 2.5×10^{-10} m^{-1} sr^{-1}. The combination of Rayleigh–Mie and potassium resonance lidar at our location enables additional temperature measurements in the mesosphere and lower thermosphere. In this configuration, the potassium lidar provides a simultaneously observed start temperature for the Rayleigh temperature calculation. We will demonstrate that this procedure avoids a bias in the upper range of the Rayleigh temperature profile (~75–90 km) that especially in summer would often result in an overestimation of the true temperature. Within NLC direct temperature measurements are inhibited by observational constraints. We describe a method to use the Rayleigh backscatter profile for the temperature calculation at least above and below the NLC. We present temperature measurements during periods with supersaturation, that are partly but not always coupled with NLC. However, every observed NLC was found at the lower edge of the supersaturated range. Our observations show that at mid-latitudes NLC are not a tracer for temperatures below the frostpoint, as similar low temperatures occur both with and without NLC.

Keywords: Mesopause region; Noctilucent clouds; Temperature; Lidar

1. Introduction

The summer mesopause region is the coldest region in the Earth's atmosphere. The temperature structure deviates strongly from the radiative mean and is characterized by wavelike structures of different scales and their influence on global circulation. In polar regions temperatures below the ice frostpoint temperature are observed for some weeks around summer solstice (Lübken, 1999; Lübken and Müllemann, 2003). Temperatures down to 120 K and less lead to the formation of ice particles, which can be observed as small, negatively charged particles by radars (described as Polar Mesosphere Summer Echoes, PMSE) and in situ instruments (see, e.g., review by Rapp and Lübken, 2004). Ice particles larger than ~10 nm are also visible by optical instruments from the ground (e.g. Hansen et al., 1989; Alpers et al., 2000; Chu et al., 2003; Höffner et al., 2003; Fiedler et al., 2005), from space (Bailey et al., 2005; DeLand et al., 2006) and by naked-eye observers (Jesse, 1885; Leslie, 1885). The optically visible ice particles are known as Noctilucent Clouds (NLC) or Polar Mesospheric Clouds (PMC).

Towards mid-latitudes NLC become increasingly rare as e.g. revealed by lidar and satellite observations (Thomas et al., 1994; von Cossart et al., 1996; Wickwar et al., 2002; Bailey et al., 2005; DeLand et al., 2006). Mean temperatures are increasing with decreasing latitude. Observations at mid-latitudes are of particular importance as trends in mesospheric temperatures may alter the occurrence of NLC especially at the edge of the typical NLC existence (Taylor et al., 2002; Thomas, 2003). At Leibniz Institute of Atmospheric Physics (IAP) at Kühlungsborn

* Corresponding author. Tel.: +49 38293 68 110; fax: +49 38293 68 50.
E-mail address: gerding@iap-kborn.de (M. Gerding).

0273-1177/$30
doi:10.1016/j.asr.2007.01.020

(54°N, 12°E) we measure temperatures by ground-based lidars from the lower troposphere up to the lower thermosphere (Alpers et al., 2004). To cover this large altitude range we operate simultaneously two co-located lidars, namely a potassium resonance lidar (K lidar) and a Rayleigh–Mie–Raman lidar (RMR lidar). Though the particular methods for lidar temperature observations are well-known for many years, to the best of our knowledge only at our site these methods are combined routinely. In particular the measurements cover the typical altitude of NLC slightly below the summer mesopause. In this paper we will describe how both lidars are combined for the benefit of noctilucent cloud, temperature, and gravity wave examination. Unfortunately, up to now no operational lidar is able to measure temperatures directly within NLC. We describe the calculation of temperature profiles above and even below the aerosol layer. We demonstrate how even the temperature observations of the RMR lidar in mesopause region do benefit from simultaneous soundings of the K lidar. The temperatures in nights with and without NLC are compared to examine the role of ambient supersaturation for NLC observations at Kühlungsborn. While the NLC soundings of the RMR lidar are performed since 1997 with up to five NLC per year, continuous temperature during NLC started not until 2003. Up to now the NLC seasons 2003–2005 are fully examined. We complement this data set by temperature profiles without NLC in 2006.

2. Instrumentation and temperature calculation

2.1. Lidar instrumentation

At Kühlungsborn the IAP operates different lidars for observations from the troposphere up to the lower thermosphere. A detailed description of the different lidars and methods used in this study can be found elsewhere (von Zahn and Höffner, 1996; Alpers et al., 2004) and shall not be repeated here in full detail. We give an update on the instrument and focus on aspects relevant for NLC and temperature measurements in the mesosphere and lower thermosphere (MLT).

The transmitter of the potassium lidar consists of an injection-seeded alexandrite ring laser operated at 770 nm. The elastic backscatter is collected by a 76-cm parabolic mirror. From the telescope the photons are guided by a quartz fiber to the detector branch. Most important parts of the detector (Fig. 1, right) are Faraday Anomalous Dispersion Optical Filters (FADOF) for daytime soundings, a narrowband interference filter, and an Avalanche Photo Diode (Fricke-Begemann et al., 2002). Beside the resonant backscatter of the K(D_1) line the elastic signal also contains molecular (Rayleigh) backscatter as well as aerosol backscatter from NLC particles.

Temperatures below the potassium layer are measured by the RMR lidar. This lidar uses a frequency-doubled

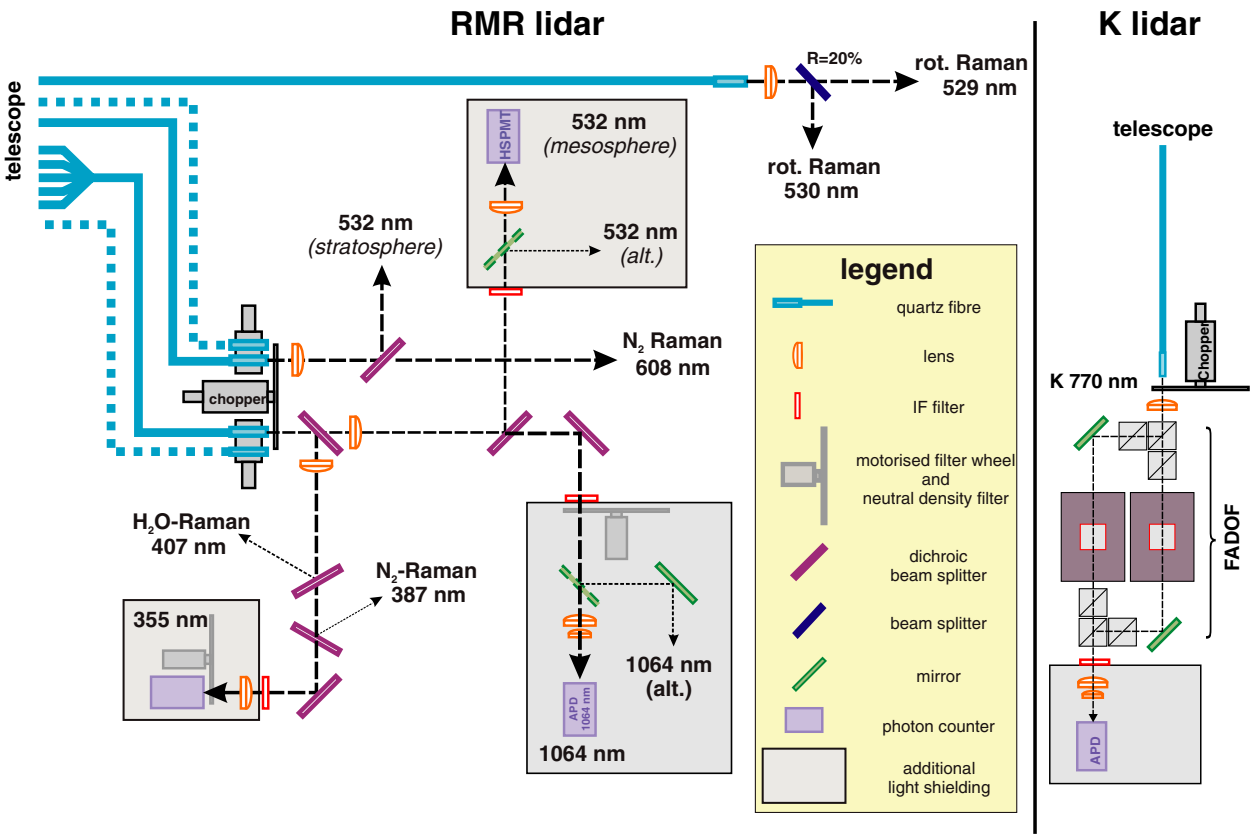

Fig. 1. Setup of the detectors of IAP Rayleigh–Mie–Raman lidar (left) and potassium resonance lidar (right). Detector channels not used in this study are only sketched. The 532 and 1064-nm channels have alternative detectors with reduced efficiency for the tropospheric soundings.

and -tripled injection-seeded Nd:YAG laser as transmitter. For temperature soundings the frequency doubled laser radiation at 532 nm is employed. For NLC soundings also the fundamental wavelength at 1064 nm and the third harmonic at 355 nm are detected (Alpers et al., 2000; Gerding et al., 2006). The backscattered photons are collected by up to seven telescopes of 50 cm diameter. For the detector branches a setup of dichroic mirrors, narrow interference filters, and photomultipliers of different sensitivity is applied. In the left part of Fig. 1 only the detector channels for NLC and mesospheric temperature soundings are shown in full detail, while the elastic and inelastic channels for tropospheric and stratospheric temperatures are only sketched.

2.2. Temperature retrieval

With the K lidar the temperature dependent Doppler broadening of the K(D_1) resonance line is examined. From the 18 wavelength channels (bin width 0.18 pm) covering the resonance line the spectral broadening is fitted in each altitude bin to yield temperature profiles with a typical integration range of 30–60 min and 1 km. As the resonance signal depends on the existence of free potassium atoms, the temperature measurement is limited to the altitude range of ~85–100 km in summer and ~80–105 km in winter (cf. Eska et al., 1998). In the altitude range below ~90 km we calculate temperatures from the air density profile (measured as a relative density profile by the Rayleigh backscatter channel at 532 nm) by integration of the hydrostatic equation. For the integration a start temperature is needed at the top of the profile, which is taken from the simultaneous observation of the K lidar at about 88 km altitude, depending on signal strength. Fig. 2 shows the advantage of simultaneously observed start temperatures compared with the use of climatological means. As described e.g. by Rauthe et al. (2006) the temperature varies in the mesopause region by about ±20 K due to gravity waves and tides. Planetary waves may induce an additional temperature shift with respect to the climatological mean. A wrong start temperature produces a bias in the calculated Rayleigh temperatures in the upper range of the profile, with the bias vanishing with decreasing altitude. Therefore, especially in the upper mesosphere a simultaneously observed start temperature provides Rayleigh temperatures with a significantly reduced systematic error. By this the data quality in the altitude range most important for NLC is significantly improved and the interpretation of the data is eased. In Fig. 2 the temperature profile as observed by the K lidar on 13 June 2006 (0:15–1:15 UT) is shown between 85 and 100 km. Especially below 90 km the observed temperatures deviate strongly from the climatological mean CIRA-86 profile (Fleming et al., 1990). Below 86 km the temperature profile derived from the RMR lidar is given with the start temperature (a) from the simultaneous sounding of the K lidar and (b) from the CIRA-86 climatology for the location of Kühlungsborn. The Rayleigh temperature is only plotted in the range where the statistical error from the Rayleigh signal plus the statistical error of the start temperature is less than 10 K. The temperature values from the K lidar and from the Rayleigh lidar (case a) agree nicely in two overlapping common altitude bins. Using the CIRA start temperature a bias of +11 K at 86 km and +5 K at 83 km exists, decreasing at lower altitude. By this the bias even exceeds the statistical uncertainty of the sounding. While the true temperature (calculated with the K lidar start temperature) is below the frostpoint temperature (T_{frost}) by up to 5 K in the range between 81 and 86 km, with the CIRA-started profile always $T \geqslant T_{frost}$ are calculated.

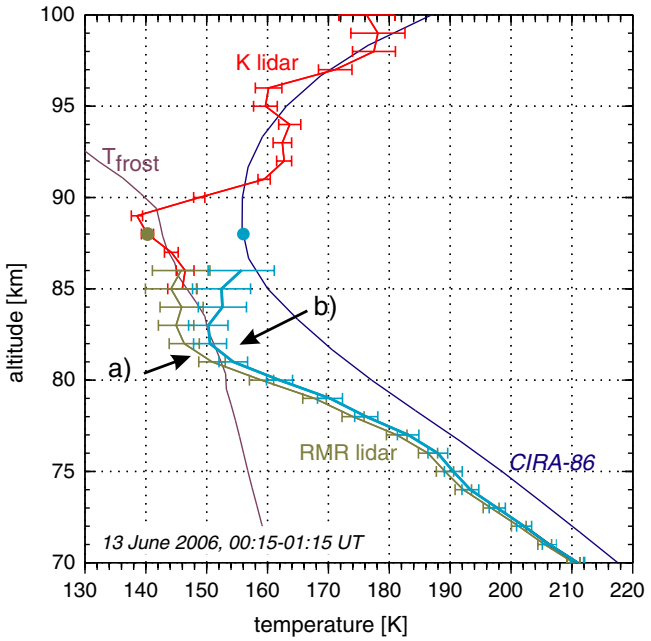

Fig. 2. Temperature profiles as observed by the RMR lidar (case a), olive green) and the K lidar (red) on 13 June 2006, 0:15–1:15 UT. The start temperature and altitude for the hydrostatic integration is marked by the olive dot. The blue line (case b) gives the temperature profile assuming a initial temperature from the CIRA-86 (blue dot). The error bars denote the statistical error in each height bin. For the CIRA-86 temperatures the statistical error is assumed as 3 K to allow comparison with the K lidar data. (For interpretation of the references to color in this figure legend, the reader is referred to the web version of this paper.)

Temperature measurements from the elastic backscatter profile require a pure molecular (Rayleigh) signal. Under the presence of NLC an additional signal from the aerosol backscatter is observed. If such a contaminated backscatter profile is accidently interpreted as true density profile, the calculated temperatures are much too low in the upper part of the NLC, and much too high below the maximum of the NLC. Fig. 3 gives an example for a NLC-contaminated backscatter profile and the related temperature profile. On 30 July 2004 a NLC was observed as a thin layer near 80 km altitude. In Fig. 3a, the green line describes the raw data profile after integration for 30 min, while the olive-green line shows the data after the interpolation described below. The interpolated profile is additionally smoothed

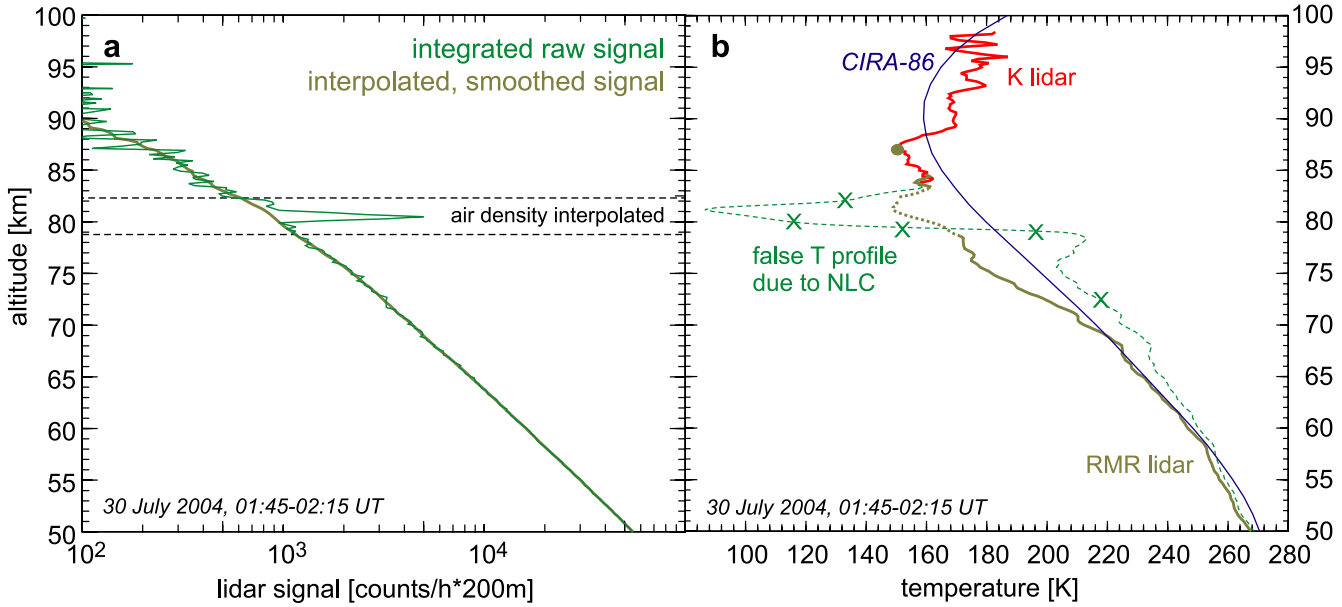

Fig. 3. Lidar backscatter profile (a) and calculated temperatures (b) during a NLC observation on 30 July 2004, 1:45–2:15 UT. Above the NLC the temperatures from interpolated and non-interpolated profiles differ only due to the smoothing algorithm. The error below the NLC decreases with altitude but remains visible even below 60 km altitude.

with an up to 3 km wide sliding average as usual for temperature calculation. In the original, non-interpolated profile the aerosol signal remains still visible even after smoothing (not shown) and results in a temperature profile as given as green dashed line in Fig. 3b. Around 80 km the calculated temperature decreases with a strongly superadiabatic gradient below 90 K, which has to be rejected without further consideration. To get the true temperature profile, we first remove the whole backscatter signal in the altitude range of the NLC. We choose one common interval for all profiles of a given NLC event (here: 78.7–82.1 km). Because we need a continuous data set for the hydrostatic integration of the density profile, we interpolate the signal in the range of the NLC with an Akima polynomial, representing discontinuous data better than e.g. typical cubic splines (Akima, 1970). After that the normal temperature calculation is performed, starting with the smoothing of the integrated raw data (cf. olive-green line in Fig. 3a). The temperature profile is affected by the gradient of the applied polynomial in the height of the NLC and due to the data smoothing also some height bins above and below. Therefore this range is considered unreliable and is rejected (cf. dashed olive-green line in Fig. 3b). Overall we are able to observe a temperature profile above and below the NLC but not directly in the altitude of the cloud. Systematic errors due to a remaining aerosol signal are avoided by a careful analysis of the calculated profiles, preventing e.g. for superadiabatic gradients in the temperature profile or sudden leaps in the time series at a particular altitude. This procedure is limited to NLC with an extension of about 2.5 km. For thicker NLC a too large part of the profile has to be removed and a temperature effect of the applied polynomial is visible even 2–5 km below the NLC. It can be shown that only NLC with a backscatter coefficient of $\beta_{532} > 0.2 \times 10^{-10}\,\mathrm{m^{-1}\,sr^{-1}}$ at 532 nm wavelength have to be considered here. Depending on shape of the NLC, very thin clouds would also alter the calculated temperature profile, but the systematic temperature error would be smaller than the statistical error in this range (~3 K).

We have tested the interpolation algorithm also with a pure molecular profile. Of course, the quality of the interpolation depends on the ambient temperature (i.e. density) profile and the width of the interpolation range. To allow for a better comparison we chose in Fig. 4 the same parameters as in the described NLC event (Fig. 3). The density profile (Fig. 4a) is interpolated between 78.7 and 82.1 km, which describes the largest interpolation range of all examined profiles in the years 2003–2005. As mentioned above, the calculated temperatures (Fig. 4b) within the interpolated range depend strongly on the polynomial used for the interpolation. These data have to be rejected. Due to the data smoothing also a ~1-km range above the interpolated region is affected. Below the interpolated range the temperature in this test case relax fast to the true observed temperatures. Therefore this "worst case" test approves the procedure applied for the profiles with NLC as a not optimal, but reliable method.

3. Case studies on temperature, supersaturation, and NLC

In this section we describe two case studies of lidar soundings during the recent summers 2005 and 2006. We will present estimations of the degree of saturation calculated from the lidar temperature data applying the vapor pressure equations of Marti and Mauersberger (1993).

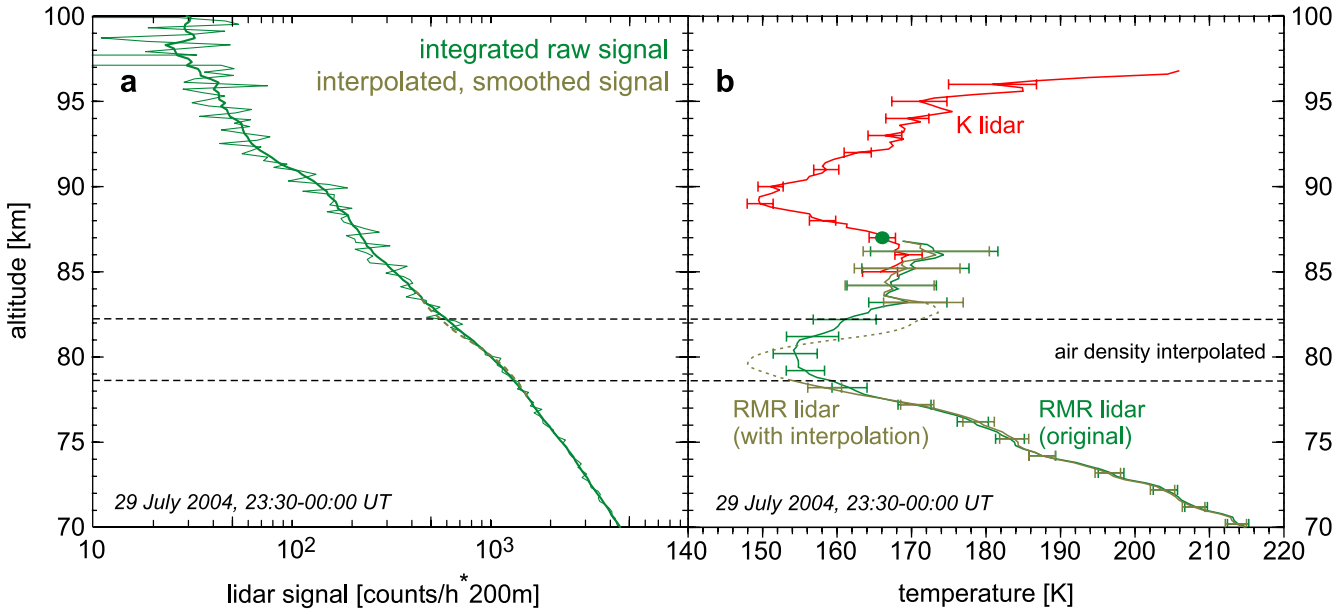

Fig. 4. Lidar backscatter profile (a) and calculated temperatures (b) on 29/30 July 2004, 23:30–0:00 UT. To test the interpolation procedure for NLC the same algorithm is applied to a profile without NLC. The original profile is shown in green (left: thin line, unsmoothed; thick line, smoothed), the profile with interpolation in olive-green. (For interpretation of the references to color in this figure legend, the reader is referred to the web version of this paper.)

The water vapor concentration is taken from the Leibniz Institute Middle Atmosphere Model (LIMA) as applied e.g. in the study of Berger and Lübken (2006). At the location of Kühlungsborn the concentration is 3–5 ppmv at 80–85 km altitude and is decreasing above. An example of the water vapor profile is presented in Gerding et al. (2006).

During the night 18/19 July 2006 we obtained temperature data for a period of ~3 h with the K lidar and for ~4 h with the RMR lidar. The temperature profiles are shown in Fig. 5a. For the temperature variability (Fig. 5b) we have subtracted the mean profile from the individual temperature data. During the first part of the

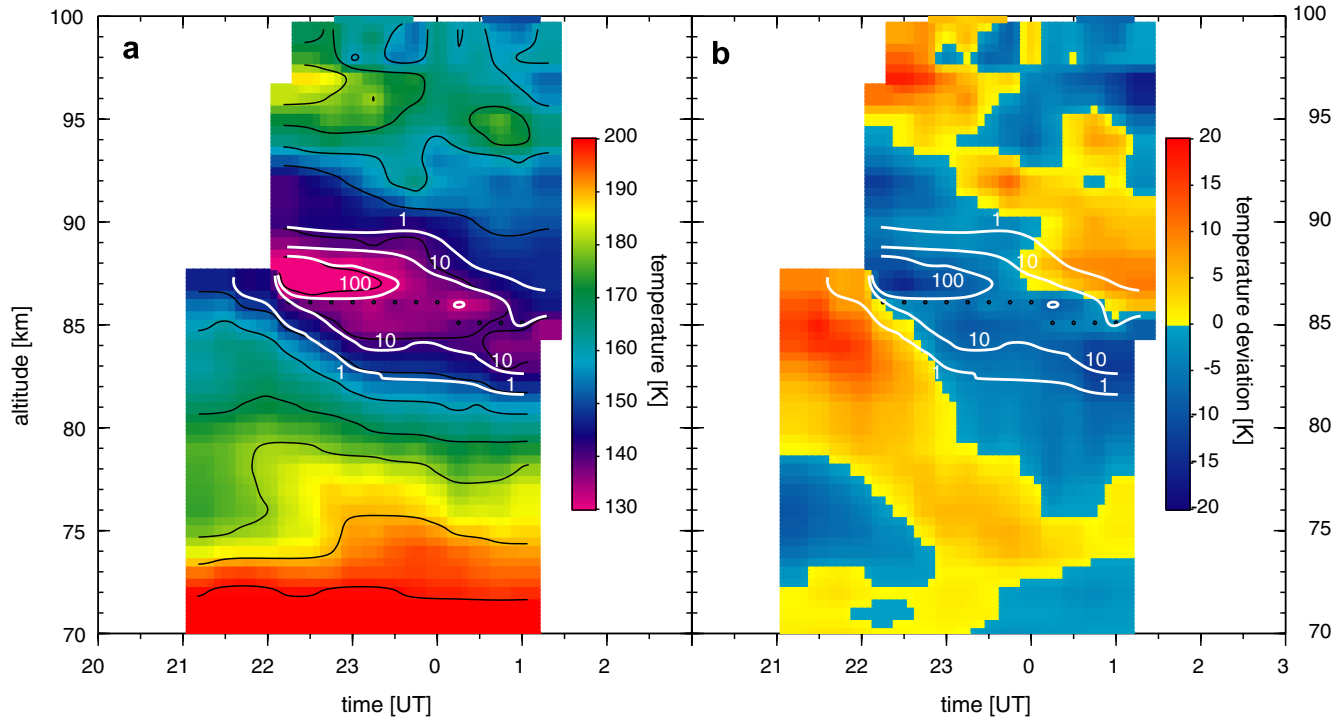

Fig. 5. Time–height cross-section of (a) temperatures and (b) temperature deviation between 70 and 100 km from the combined soundings of K lidar and RMR lidar during the night 18/19 July 2006. The saturation ratio is given in white contour lines using water vapor concentrations from the LIMA model.

observation the temperature was lower than 125 K at 87 km, yielding a degree of saturation of $S > 100$. Overall, the temperatures are below the frost point in an altitude range of 6 km width. The supersaturated range descends with time by about 5 km, i.e. with an absolute phase speed of $\sim$1.5 km h^{-1}. Fig. 5b, demonstrates the high variability of temperatures due to gravity waves above our site. The temperature varies by more than 20 K within about 3 h of observation, as it is found typical for our observations (Rauthe et al., 2006). It should be noted that the observed gravity wave phases descend much faster with -3 to -4 km h^{-1}. During the whole time of the sounding no NLC was detected by the lidars, despite this high supersaturation. Also the co-located OSWIN radar did not observe any mesospheric summer echo (MSE) in the morning hours (M. Zecha, private communication, 2006) (At night the OSWIN radar usually does not detect MSE due to low electron concentration, but MSE may appear in the early morning when the electron concentration rises again due to illumination by the sun.). Visible observations by an automated CCD-camera at our institute proved that during the lidar soundings a NLC existed less than 300 km northward of our location.

In a second case study we describe the observations during the night 13/14 June 2005. Within this night we obtained temperature data by the K lidar for about 5.5 h and by the RMR lidar for about 4 h (Fig. 6). In the beginning of the night local temperature minima of 135 and 142 K have been observed around 84 and 91 km, respectively. In a layer between 83 and 86 km the temperatures were below the frost point. Even saturation ratios of $S > 10$ are observed temporarily. The upper cold layer descended during the night while the lower one remained nearly constant with height but became warmer. Eventually, when the upper layer went below 89 km at about 23:30 UT it also became supersaturated, with temperatures decreasing further below 140 K around 87 km altitude. A NLC appeared at 0:05 UT in the lidar backscatter signal. At about the same time the lower edge of the upper supersaturated layer reached an altitude of 85 km. The lower supersaturated region extended up to 84 km in the last continuous profile (not affected by the NLC). This gives reason for the assumption that both supersaturated layers have merged. The NLC was observed for about 1 h by both lidars at 770, 532, and 355 nm. The backscatter coefficient β_{532} reached a maximum value of more than 5×10^{-10} m^{-1} sr^{-1}, which describes a comparatively strong NLC at our mid-latitude location (cf. Gerding et al., 2006).

The presented case studies show that NLC appear above our location during periods of supersaturation. But supersaturation is by far not sufficient for the existence of ice particles that are large enough to be observed by lidar or for the existence of ice particles at all. Gerding et al. (2006) describe several cases with NLC appearing at the lower edge of a supersaturated region. All available wind profiles during NLC show southward wind in this particular height region, typically also several hours before the NLC was observed. On the other hand Gerding et al. (2006) claim that NLC are observed in only 20% of all nights with $T < T_{\text{frost}}$ at altitudes below 85 km. This underlines the important role of advection of NLC particles for the observation of NLC above Kühlungsborn.

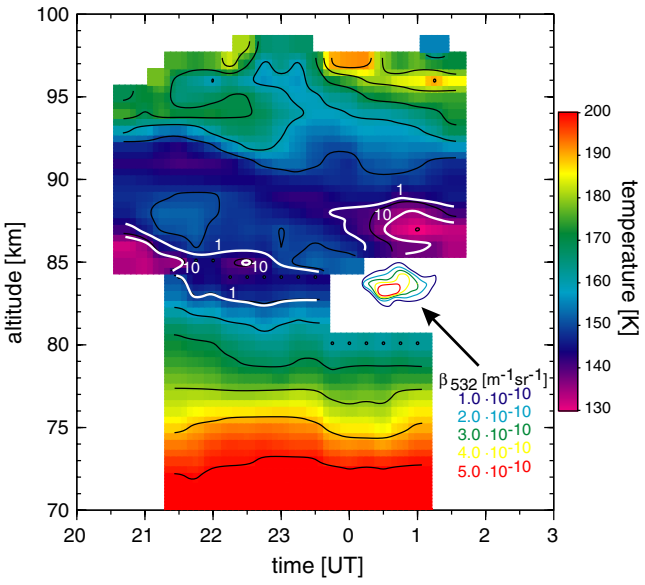

Fig. 6. Time–height cross-section of temperatures between 70 and 100 km from the combined soundings of K lidar and RMR lidar during the night 13/14 June 2005. The saturation ratio is given in white contour lines using water vapor concentrations from the LIMA model. The colored contour lines show the NLC backscatter coefficient at 532 nm. (For interpretation of the references to color in this figure legend, the reader is referred to the web version of this paper.)

4. Mean profiles of saturation

In the previous section we have shown that ambient supersaturation is not sufficient for the existence of NLC, i.e. that there are mutually no differences in the time-dependent data sets with and without NLC. Here we describe the night mean profiles of saturation during the months June/July of the years 2003–2005 to examine potential differences of the mean atmospheric state of nights with and without NLC. We have calculated night mean temperature profiles based on 3–5 h of observation per night. By this procedure we average across short-scale gravity waves with periods shorter than $\sim$3 h. However, this procedure will not affect our main results as the shorter waves are more likely to destroy NLC than to produce new ones (Klostermeyer, 1998; Rapp et al., 2002). From the temperature profiles an average saturation profile is calculated. For the comparison only the degree of saturation in each individual height bin (1 km width) is of interest, but not the variation with altitude in a single night. In Fig. 7 we have plotted five nights with NLC in blue color and 29 nights without NLC are plotted in grey. Within the period June/July several warm nights have been observed, showing no supersaturation at all. However, we would like to concentrate on the nights with $T < T_{\text{frost}}$ ($S > 1$) as only these allow the

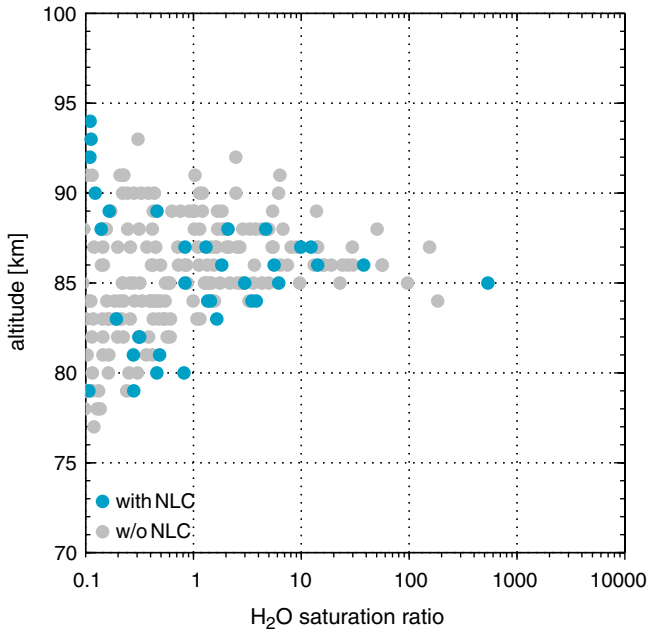

Fig. 7. Degree of water vapor saturation from the nightly mean temperatures of all observations during June/July of the years 2003–2005. The individual data points are shown with 1 km resolution. Data points from NLC-nights are colored in blue. (For interpretation of the references to color in this figure legend, the reader is referred to the web version of this paper.)

existence of ice particles. Part of the NLC nights show height ranges without supersaturation, but we have to note, that these ranges are below the NLC or several kilometers above. Again, here the points with the largest degrees of saturation are the most important ones, as they describe the maximum of supersaturation.

The highest degrees of saturation are observed in the region between 85 and 90 km. Saturation ratios of $S > 10$ in the nightly mean are in general limited to altitudes above 85 km, while below 85 km the degree of saturation is typically less than 10 and partly less than 1. The most important fact is the observation of very high degrees of saturation in both kind of data, with and without NLC. Even the observation of very high saturation ratios is not sufficient for the detection of an accompanying NLC. Of course, the mean saturation ratio of all NLC nights is somewhat higher than the mean ratio of non-NLC nights. But this is not surprising as the mean temperature at our location is in general higher than the frost point temperature and NLC are limited to the colder-than-average nights (Gerding et al., 2006).

5. Discussion

Up to now there is only a limited number of temperature soundings in summer, covering the whole altitude region of 70–90 km with a comparable or better altitude resolution. All these soundings are in situ measurements performed at higher latitudes (e.g. Philbrick et al., 1984; Rapp et al., 2002; Lübken et al., 2004) while satellite soundings suffer e.g. from coarser altitude resolutions. Lidar observations are typically performed above or below NLC, but not at the same time above and below the ice cloud (Hansen and von Zahn, 1994; Collins et al., 2003). The lidar soundings show $T < T_{\text{frost}}$ above the NLC and $T > T_{\text{frost}}$ below. In situ measurements at polar latitudes confirm the observation of NLC at the lower edge of the supersaturated range. Some of the soundings reveal also supersaturation without accompanying NLC, but typically these measurements describe no temporal evolution. Therefore the duration of supersaturation is unknown.

We have presented an example with temperatures much below the ice frost point (Fig. 5). From our limited data set we can only speculate on the reasons that inhibited the formation of ice particles: Gerding et al. (2006) describe that the existence of NLC is limited to the cold phases of waves and tides. During 18/19 July 2006 the period with supersaturation may have been too short for the formation of NLC particles. E.g. Rapp et al. (2002) suggest 4–6 h until new particles are grown to lidar-visible size. The possible influence of the ambient wind field on NLC observations at Kühlungsborn is discussed by Gerding et al. (2006). Additionally, all scenarios of NLC formation require the existence of condensation nuclei, what can not be proven (or rejected) by our observations.

We further do not want to conceal that our study uses some assumptions on poorly known quantities. In particular there is still a strong need for accurate time-dependent and high-resolved measurements of water vapor concentration. Berger and Lübken (2006) describe the model study of the variability of water vapor due to transport processes in the mesopause region and freeze-drying by NLC. For our study we used water vapor concentrations of ~3–5 ppmv in the altitude range below 85 km, decreasing above down to ~1 ppmv at 90 km. For the lower part this number is in the range of the available measurements (e.g. Nedoluha et al., 2000). Further we remark that if the true water vapor concentration above 85 km is higher than assumed here also the true degree of saturation is higher. By this, e.g. the number of supersaturated cases without NLC would increase even more.

We use the vapor pressure equation of Marti and Mauersberger (1993) as e.g. suggested by Rapp and Thomas (2006). From our observation we can not decide whether this equation or the concurrent one of Mauersberger and Krankowsky (2003) is correct, as both equations give similar results at $T \approx T_{\text{frost}}$ and deviate strongly at $T \ll T_{\text{frost}}$. But the equation of Mauersberger and Krankowsky (2003) would confirm our results and, even more, would result in much higher saturation ratios at very low temperatures.

6. Summary and conclusions

We have shown that temperatures profiles are obtained by lidar in the altitude range up to ~100 km even in the presence of NLC. As we can not distinguish with the RMR lidar between aerosol and molecular elastic

scattering, the temperatures within NLC remain hidden from our observations. But for NLC with a thickness of up to ~2.5 km temperature measurements just above and below the NLC are performed at our station and provide valuable information e.g. on the degree of water vapor saturation in the vicinity of NLC. The retrieval depends crucial on the existence of time-dependent temperature data for the start value of the hydrostatic integration, as an error in the start temperature induce a bias in the temperature data below. Time-dependent temperature data exist for our station from simultaneous, co-located soundings of the K lidar. These observations prove the high variability of temperatures in the mesopause region. We have demonstrated that the use of this data as start values of the Rayleigh temperatures remove some systematic uncertainty induced by climatological mean start values.

A case study representative for all our observations revealed the NLC at the lower edge of a supersaturated region. While this is expected from model results and high-latitude soundings, it is now confirmed for the first time at a mid-latitude station. None of our soundings give evidence for already sublimating NLC ($S < 1$). On the other side we described an event with supersaturation but without NLC. This case is in fact representative for the majority of nights were we observe temperatures below the frost point but no NLC. Our soundings support time constants of more than about 4–6 h necessary for the formation of NLC. These times are typically larger than the periods of supersaturation within the cold phases of gravity waves and tides. Therefore, NLC observations at our side depend strongly on the advection of ice particles from polar latitudes. Air parcels with and without NLC that are advected to our site do not differ in terms of mean temperature. As a general conclusion from our observations we revealed a de-coupling of NLC-existence from both the ambient time-dependent and mean temperature. The usage of NLC-extension as a proxy for climate trends requires further studies e.g. on changes in the advection of ice particles, i.e. on the meridional wind field.

Acknowledgments

We thank our colleagues at IAP and numerous summer students for their help in the nighttime lidar soundings. T. Köpnick and M. Priester did valuable work in lidar operation and maintenance. Provision of LIMA data by U. Berger is gratefully acknowledged. Part of this work was supported by the Deutsche Forschungsgemeinschaft (DFG) under Grant GE1625/1-1.

References

Akima, H. A new method of interpolation and smooth curve fitting based on local procedures. J. Ass. Comp. Mach. 17, 589–602, 1970.

Alpers, M., Gerding, M., Höffner, J., von Zahn, U. NLC particle properties from a five-color lidar observation at 54°N. J. Geophys. Res. 105 (D10), 12235–12240, 2000.

Alpers, M., Eixmann, R., Fricke-Begemann, C., Gerding, M., Höffner, J. Temperature lidar measurements from 1 to 105 km altitude using resonance, Rayleigh, and rotational Raman scattering. Atmos. Chem. Phys. 4 (3), 793–800, 2004.

Bailey, S.M., Merkel, A.W., Thomas, G.E., Carstens, J.N. Observations of polar mesospheric clouds by the Student Nitric Oxide Explorer. J. Geophys. Res. 110, D13203, doi:10.1029/2004JD00542, 2005.

Berger, U., Lübken, F.-J. Weather in mesospheric ice layers. Geophys. Res. Lett. 33, L04806, doi:10.1029/2005GL02484, 2006.

Chu, X., Gardner, C.S., Roble, R.G. Lidar studies of interannual, seasonal, and diurnal variations of polar mesospheric clouds at the south pole. J. Geophys. Res. 108 (D8), 8447, doi:10.1029/2002JD00252, 2003.

Collins, R.L., Kelley, M.C., Nicolls, M.J., Ramos, C., Hou, T., Stern, T.E., Mizutani, K., Itabe, T. Simultaneous lidar observations of a noctilucent cloud and an internal wave in the polar mesosphere. J. Geophys. Res., 108. ACL 2–1/7, 2003.

DeLand, M.T., Shettle, E.P., Thomas, G.E., Olivero, J.J. A quarter-century of satellite polar mesospheric cloud observations. J. Atmos. Sol. Terr. Phys. 68 (1), 9–29, 2006.

Eska, V., Höffner, J., von Zahn, U. Upper atmosphere potassium layer and its seasonal variations at 54°N. J. Geophys. Res. 103 (A12), 29207–29214, 1998.

Fiedler, J., Baumgarten, G., von Cossart, G. Mean diurnal variations of noctilucent clouds during 7 years of lidar observations at ALOMAR. Ann. Geophys. 23 (4), 1175–1181, 2005.

Fleming, E.L., Chandra, S., Barnett, J.J., Corney, M. Zonal mean temperature, pressure, zonal wind, and geopotential height as functions of latitude. Adv. Space Res. 10, 11–59, 1990.

Fricke-Begemann, C., Alpers, M., Höffner, J. Daylight rejection with a new receiver for potassium resonance temperature lidars. Opt. Lett. 27 (21), 1932–1934, 2002.

Gerding, M., Höffner, J., Rauthe, M., Singer, W., Zecha, M., Lübken, F.-J. Simultaneous observation of NLC, MSE and temperature at a mid-latitude station (54°N). J. Geophys. Res., submitted for publication, doi:10.1029/2006JD008135, 2006.

Hansen, U., von Zahn, G. Simulataneous observations of noctilucent clouds and mesopause temperatures by lidar. J. Geophys. Res. 99 (D9), 18989–18999, 1994.

Hansen, G., Serwazi, M., von Zahn, U. First detection of a noctilucent cloud by lidar. Geophys. Res. Lett. 16 (12), 1445–1448, 1989.

Höffner, J., Fricke-Begemann, C., Lübken, F.-J. First observations of noctilucent clouds by lidar at Svalbard, 78°N. Atmos. Chem. Phys. 3, 1101–1111, 2003.

Jesse, O. Auffallende Abenderscheinungen am Himmel. Meteor. Z. 2, 311–312, 1885.

Klostermeyer, J. A simple model of the ice particle size distribution in noctilucent clouds. J. Geophys. Res. 103 (D22), 28743–28752, 1998.

Leslie, R.C. Sky glows. Nature 32, 245, 1885.

Lübken, F.-J. Thermal structure of the Arctic summer mesosphere. J. Geophys. Res. 104 (D8), 9135–9149, 1999.

Lübken, F.-J., Müllemann, A. First in situ temperature measurements in the summer mesosphere at very high latitudes (78°N). J. Geophys. Res. 108 (D8), 8448, doi:10.1029/2002JD00241, 2003.

Lübken, F.-J., Zecha, M., Höffner, J., Röttger, J. Temperatures, polar mesosphere summer echoes, and noctilucent clouds over Spitsbergen (78°N). J. Geophys. Res. 109 (D11), D11203, doi:10.1029/2003JD00424, 2004.

Marti, J., Mauersberger, K. A survey and new measurements of ice vapor pressure at temperatures between 170 and 250 K. Geophys. Res. Lett. 20, 363–366, 1993.

Mauersberger, K., Krankowsky, D. Vapor pressure above ice at temperatures below 170 K. Geophys. Res. Lett. 30 (3), doi:10.1029/2002GL01618, 21/1-3, 2003.

Nedoluha, G.E., Bevilacqua, R.M., Gomez, R.M., Hicks, B.C., Russell III, J.M., Connor, B.J. Ground-based microwave observations of middle atmospheric water vapor in the 1990s, in: Siskind, D.E., Eckermann, S.D., Summers, M.E. (Eds.), Atmospheric Science across

the stratopause, vol. 123 of Geophysical Monograph, American Geophysical Union, Washington DC, USA, pp. 257–270, 2000.

Philbrick, C.R., Barnett, J., Gerndt, R., Offermann, D., Pendleton, W.R., Schlyter, P., Schmidlin, F.J., Witt, G. Temperature measurements during the CAMP program. Adv. Space Res. 4 (4), 153–156, 1984.

Rapp, M., Lübken, F.-J. Polar mesosphere summer echoes (PMSE): review of observations and current understanding. Atmos. Chem. Phys. 4, 2601–2633, 2004.

Rapp, M., Thomas, G.E. Modeling the microphysics of mesospheric ice particles: assessment of current capabilities and basic sensitivities. J. Atmos. Sol. Terr. Phys. 68 (7), 715–744, 2006.

Rapp, M., Lübken, F.-J., Müllemann, A., Thomas, G.E., Jensen, E. Small-scale temperature variations in the vicinity of NLC: experimental and model results. J. Geophys. Res. 107 (D19), 4392, doi:10.1029/2001JD00124, 2002.

Rauthe, M., Gerding, M., Höffner, J., Lübken, F.-J. Lidar temperature measurements of gravity waves over Kühlungsborn (54°N) from 1 to 105 km: A winter–summer comparison. J. Geophys. Res. 111 (D24), D24108, doi:10.1029/2006JD00735, 2006.

Taylor, M.J., Gadsden, M., Lowe, R.P., Zalcik, M.S., Brausch, J. Mesospheric cloud observations at unusually low latitudes. J. Atmos. Sol. Terr. Phys. 64, 991–999, 2002.

Thomas, G.E. Are noctilucent clouds harbingers of global change in the middle atmosphere? Adv. Space Res. 32 (9), 1737–1746, 2003.

Thomas, L., Marsh, A.K.P., Wareing, D.P., Hassan, M.A. Lidar observations of ice crystals associated with noctilucent clouds at middle latitudes. Geophys. Res. Lett. 21 (5), 385–388, 1994.

von Cossart, G., Hoffmann, P., von Zahn, U., Keckhut, P., Hauchecorne, A. Mid-latitude noctilucent cloud observations by lidar. Geophys. Res. Lett. 23 (21), 2919–2922, 1996.

von Zahn, U., Höffner, J. Mesopause temperature profiling by potassium lidar. Geophys. Res. Lett. 23 (2), 141–144, 1996.

Wickwar, V.B., Taylor, M.J., Herron, J.P., Martineau, B.A. Visual and lidar observations of noctilucent clouds above Logan, Utah, at 41.7°N. J. Geophys. Res. 107 (D7), doi:10.1029/2001JD00118. ACL 2/1–7, 2002.